Irradiation and temperature dependency of the contact resistances in silicon solar cells based on measurement and simulation comparison

Vera van de Ven
Integrated Devices and Systems (IDS)
University of Twente
Enschede, The Netherlands
November 2024

***Abstract*—The use of solar panels is increasing as the world is moving towards a more sustainable way of using energy. To improve the efficiency of these solar cells the effects of environmental factors are investigated so the circumstances for maximum power output can be found. In this paper, the effect of irradiation and temperature on the contact resistances is examined. Temperature, for example, changes important parameters such as the bandgap energy and the mobility of carriers in the semiconductor material. As the focus is on contact resistances these are first characterised using the transmission line method (TLM). An equivalent model is used to further investigate the effect of changing parameters as increasing irradiation and nonidealities like extra current paths. Theoretical analysis shows that there is an optimal temperature range for the solar cell at which the internal material resistances are lowest. Results show that irradiation decreases the contact resistance. A specific relation is not found as shunt resistances greatly affect the outcome of measurements.**

I. Introduction

As climate change becomes an increasingly prominent topic of discussion, the demand for renewable energy sources is growing. Since 2015 the use of renewable energy sources in the Netherlands almost tripled. Examples of renewable energy sources are wind, biomass, and solar energy. The latter being the largest growing renewable energy source over the last couple of years with an increase of 17% compared to 2022 [1]. The increase in accessibility of solar panels for households partially causes this. To improve the power obtained from these panels, it is interesting to research what effects improve or deteriorate the current flow in such a cell.

As we are interested in a higher current flow a smaller resistance is preferable. This paper will focus on characterizing the contact resistances of a silicon solar cell with an aluminium backside field, specifically looking at the influence of the irradiation intensity and temperature. These influences on the contact resistances are found by comparing actual measurements to the results of a simulated equivalent model. Answering the research question: '*What is the influence of irradiation and temperature on the behaviour of contact resistances comparing simulation and measurement?*' will summarize this paper.

In previous experimental studies, [2], it was found that irradiation and temperature affect the results from the Transmission Line Method (TLM). TLM is used to characterize the contact resistances in a solar cell. A nonlinear relation between the irradiation intensity and the contact resistance was found, along with a linear relation between the contact resistance and the temperature of the cell. [3] shows that the relation between the contact resistance and irradiation intensity is strongly influenced by the doping of the semiconductor. The trustworthiness of the results in [3] is however questioned as contradicting results were obtained from different simulations. Hence the hypothesis is that relations regarding the contact resistances found in this experimental study are closer to the ones found in [2].

Solar panels are used in a wide range of weather conditions which results in a lot of variable parameters that can influence the current flow in the solar cell. To scale down the complexity of this experimental study, the number of variable parameters is reduced. This is done by testing in a controlled environment, the temperature is constant and the irradiation intensity can be adjusted as needed. As material characteristics and production processes may differ per cell type is the focus on only one specific cell.

The next section will provide the theory about the current generation in solar cells, the equivalent model and how material properties change parameters. Following in the same section the measurement setup is described, after which the new section provides the results of these measurements. In the last part of this report, the simulation results of different iterations of ideality are compared. Finishing this research with a conclusion where all results and improvements are summarized.

II. Analysis and Method

To create an equivalent circuit model of a solar cell, the physics of the current generation in a cell and the components used to model its behaviour must be understood. This section provides the knowledge needed to predict the temperature and irradiation influence in the solar cell.

A. Current Generation in a solar cell

Current generation in solar cells is based on the separation of electron-hole pairs in the depletion layer between the doped regions. When light hits the depletion layer, electron-hole pairs are separated. An electron is excited from the valence band to the conduction band. The irradiation wavelength needed to excite an electron is inversely proportional to the bandgap energy. In this report, the effect of the irradiation wavelength on the current generation is not investigated, as this is out of the scope of the main research goal. Due to an induced electric field in the pn-junction electrons and holes get accelerated in different directions creating a current. The amount of current generated in the cell, the photo current (I_{ph}), is directly proportional to the amount of irradiation on the cell, as with more light more electrons get excited resulting in a bigger current flow. The energy needed to excite an electron from the valence to the conduction band is dependent on the bandgap energy (E_g). A smaller bandgap would indicate that less energy is needed to excite the same amount of electrons, creating the same flow of current. The dependence of the bandgap energy on temperature can be described by eq. 1 [4]. Where the temperature *(T)* is given in [K], the bandgap energy (E_g) of silicon is typically 1.12 [eV] at 300 [K] and a value of -2.3×10^{-4} [$\frac{eV}{K}$] is normal for $\frac{dE_g}{dT}$ [5]. In Fig. 1 the bandgap energy of silicon is plotted for the temperature which ranges from 273 [K] to 313 [K], a decrease is [eV] can be observed.

$$E_g(T) = E_g(300K) + \frac{dE_g}{dT}(T - 300) \quad (1)$$

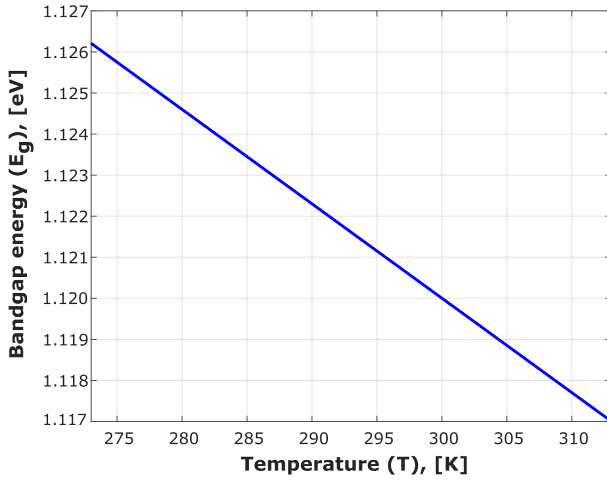

Fig. 1: Visualization of eq. 1, the bandgap energy of silicon in [eV] versus the temperature in [K].

The amount of current flow in the solar cell assuming there is no early recombination can be described by eq. 2. The equation is derived from the shockley ideal diode equation, in combination with Kirchhoff's laws and Ohm's law. The current measured over the cell is the photo current (I_{ph}) minus the current through the series and shunt resistors of the diode [4].

$$I = I_{ph} - \frac{V + IR_s}{R_{shunt}} - I_s[e^{\frac{V+IR_s}{nV_{th}}} - 1] \quad (2)$$

V_{th} is the thermal voltage in [V], R_s and R_{shunt} are the series and shunt resistance in [Ω] for the diode model respectively. As I_{ph} increases due to an increase in irradiation intensity, as previously described in this section, the current measured also increases. The temperature influence is seen in the diode current, where the thermal voltage is given as a variable in the exponent. The thermal voltage can be described by: $V_{th} = \frac{k_B T}{q}$, where k_B is the Boltzmann constant is 1.38 $\times 10^{-23}$ in [$\frac{J}{K}$], q is the elementary charge of 1.602 $\times 10^{-19}$ [C]. As the temperature increases, the exponent, for the diode current decreases resulting in a smaller value multiplied with I_s resulting in a smaller value that is subtracted from the photon current.

1) Back surface field: One of the ways to improve the efficiency of a solar cell is by introducing a back surface field (BSF). This is a thin coating at the back side of the solar cell preventing premature recombination. By introducing an electric field the minority carriers are repelled at the back side of the cell. The strength of the electric field formed is proportional to the aluminium doping concentration in the silicon [6]. Early recombination would reduce the number of generated free carriers thereby bringing down the effective current. In the case of the solar cell examined in this paper, the material used is aluminium. It is assumed that because of the electric field at the back side of the cell there is no extra recombination at the back side of the cell and therefore no extra losses are taken into account.

B. Equivalent model

To predict and compare the behaviour of a solar cell, an equivalent lumped element model is created. The simplest form consists of a few resistors and two diodes. Since it is a lumped element model, the model can be extended in the hope of predicting the continuous behaviour of the solar cell more accurately. The n-doped layer and a p-doped layer in the solar cell can be modelled using a diode. Internal material resistances and the Schottky contact between the silver contact strips on top of the cell and the substrate are modelled with resistors. In Fig. 2, it is shown how the model compares to the cross-section of the solar cell.

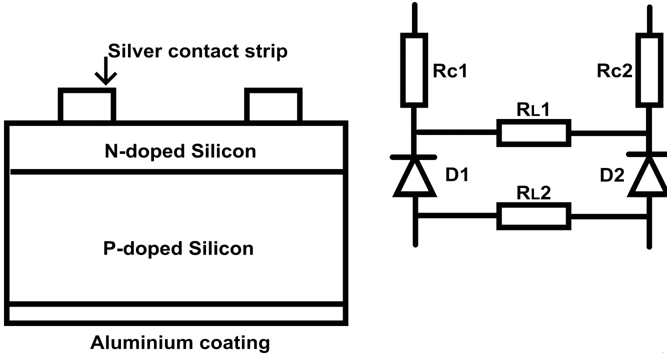

Fig. 2: Left: vertical cross-section of a solar cell where the differently doped silicon layers, aluminium coating and silver contacts can be seen, right: the equivalent lumped element model of the vertical cross-section of the solar cell.

1) Resistance: In the ideal model, two types of resistances can be defined: the sheet resistance, which is a material property, and the contact resistance which is a Schottky contact between the silver contact strips on top of the cell and the silicon. The internal metal resistance of the silver contact strips is assumed to be negligible due to its high conductive properties and the resistance of the aluminium BSF is also neglected.

The sheet resistivity (ρ_{sheet} $[\Omega \cdot cm]$) can be calculated from eq. 3, where σ is the conductivity in $[\frac{1}{\Omega \cdot cm}]$, n and p are the electron and hole carrier densities in $[cm^3]$, q is the elementary charge of 1.602×10^{-19} [C], and μ_e and μ_h are the electron and hole mobilities in $[\frac{cm^2}{V \cdot s}]$ respectively [7].

$$\rho_{sheet} = \frac{1}{\sigma} = \frac{1}{nq\mu_e + pq\mu_h} \quad (3)$$

μ_e and μ_h of silicon are both temperature and doping concentration dependent and approcimated by eq. 4 and eq. 5 [8].

$$\mu_e = 88(\frac{T}{300})^{-0.57} + \frac{7.4 \times 10^8 \times T^{-2.33}}{1 + 0.88(\frac{N_d}{1.26 \times 10^{17} \times (\frac{T}{300})^{2.4}})(\frac{T}{300})^{-0.146}} \quad (4)$$

$$\mu_h = 54.3(\frac{T}{300})^{-0.57} + \frac{1.36 \times 10^8 \times T^{-2.33}}{1 + 0.88(\frac{N_d}{2.35 \times 10^{17} \times (\frac{T}{300})^{2.4}})(\frac{T}{300})^{-0.146}} \quad (5)$$

The hole and electron carrier densities (*n, p*) are also temperature dependent as seen in eq. 6 and eq. 7. N_c and N_V are the effective densities of the conductance and valence band in $[\frac{1}{cm^3}]$. The Boltzmann constant (k_B) is 1.38×10^{-23} $[\frac{J}{K}]$.

$$n = N_C(\frac{T}{300})^{\frac{3}{2}} \exp(\frac{E_F - E_c}{k_B T}) \quad (6)$$

$$p = N_V(\frac{T}{300})^{\frac{3}{2}} \exp(\frac{E_V - E_F}{k_B T}) \quad (7)$$

From Fig. 3 the temperature dependence of the conductivity is seen, the doping concentration are estimations based on [9]. There is an acceptor doping of 6.6×10^{15} $[\frac{1}{cm^3}]$ or a donor doping of 1×10^{18} $[\frac{1}{cm^3}]$.

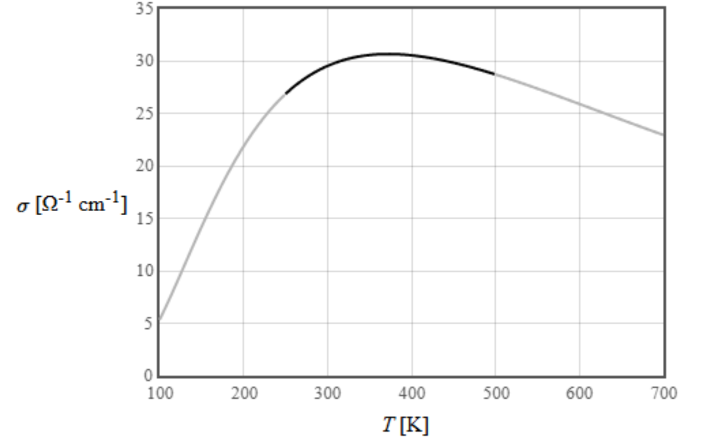

Fig. 3: Temperature dependence of the conductivity of silicon for an acceptor doping (N_a) of 6.6×10^{15} $[\frac{1}{cm^3}]$ or a donor doping (N_d) of 1×10^{18} $[\frac{1}{cm^3}]$ [7].

The sheet resistance is area dependent. As the exact depth of the silicon layers is not known the effective sheet resistivity will be expressed in $[\Omega/[\square]]$, a unit that describes the resistivity of a material independent of area. The ratio of the resistances for the n- and the p-doped layers of silicon is, for now, estimated at 1:5.

The contact resistance is the resistance from the Metal-Semiconductor junction on top of the cell formed by the silver contact strips and doped silicon. Looking at the band diagram of a semiconductor, there are no energy states available for electrons between the valence and conductance band. In Fig. 4 this is shown as the lighter grey area between E_C and E_V, metal does not have such a forbidden band gap. Band bending occurs as the materials make contact. As the contact is in thermal equilibrium the Fermi levels align.

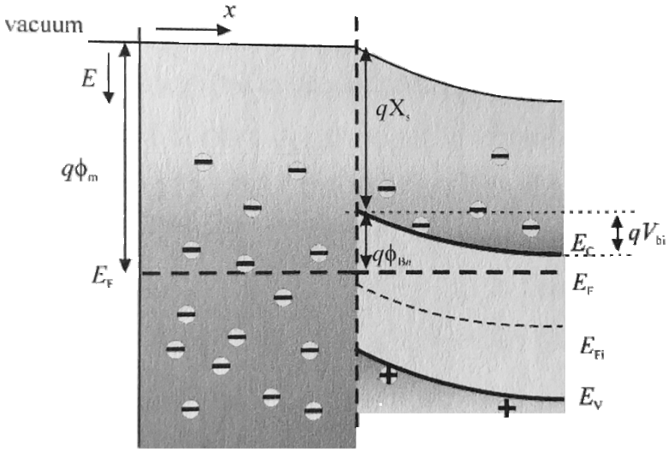

Fig. 4: Banddiagram of a Metal-Semiconductor junction at thermal equilibrium [10].

Depending on the doping of the n-type semiconductor, there is thermionic emission, field emission, or both. For a low doping concentration in the semiconductor, there will be thermionic emission. Thermionic emission means that electrons are thermally 'excited' to overcome the barrier created by band bending, causing a current to flow. As the doping increases to an intermediate doping concentration, both thermionic and field emission will take place. For high doping concentrations in the semiconductor the barrier between the metal and semiconductor is narrow enough that electrons can tunnel through [11]. So depending on the concentration of the n-doped layer, the temperature will influence how easily electrons will be able to flow in the contact.

The contact resistance measured is dependent on the area of the contacts [2]. ρ_{c-eff} is the effective specific contact resistance in $[\Omega \cdot cm^2]$ and can be found using eq. 8, where L and Z are the length and width of the contact in [cm] and R_C is the measured contact resistance in $[\Omega]$. This simplified equation can be used since $W \leq 0.5L_T$. L_T is the transfer length, which is the average distance over which the most electrons exit or enter the metal-semiconductor contact. The transfer lenght can be found by dividing the y intersection by 2 from the total distance versus total resistance plot.

For the sample used to characterise the contact resistances $Z = 2 \times 10^{-2}$ [cm] and $L = 1.5$ [cm].

$$\rho_{c-eff} = R_C L Z \tag{8}$$

For simplicity reasons the contact is assumed to have linear IV characteristics and is therefore modelled as a regular resistor.

2) Diode: The diode used in the equivalent model represents the junction between the n- and p-doped silicon in the solar cell. Based on the Shockley ideal diode equation, $I = I_s(e^{\frac{qV}{nk_bT}} - 1)$, it can be seen that for an increasing temperature with a set voltage, the maximum current is lower. For this equation is I the current in [A], I_s is the saturation current in [A], V is the voltage applied to a diode in [V], n is the ideality factor describing how 'perfect' the diode behaves as a diode (in case of an ideal diode n = 1). As the ideality factor grows, the amount of current leaking after the threshold voltage decreases, this is seen in Fig. 5.

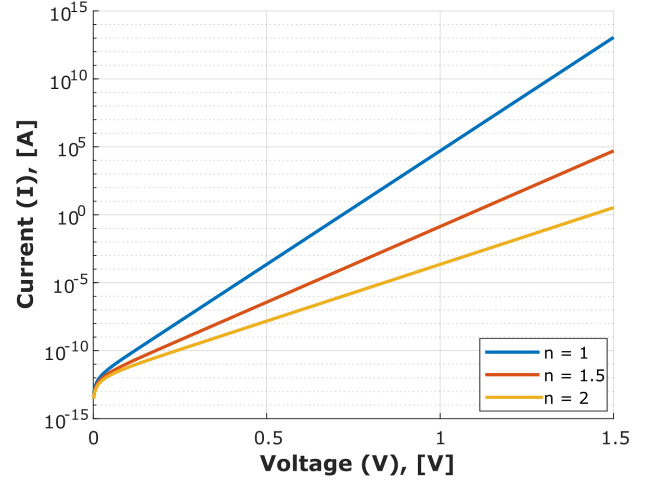

Fig. 5: Current through a diode for different values of the ideality factor (n).

The saturation current, a constant in the Shockley diode equation, is of great influence on the current measured through the diode. The saturation current is a combination of the diffusion current caused by minority carriers and a generation current formed in the depletion layer of the pn-junction. The temperature dependence of the saturation current can be approximated by eq. 9 [12].

$$I_s = [constants] \times e^{\frac{-E_g}{xkT}} \tag{9}$$

Where x is a value between 1 and 2 depending on which type of current generation is most dominant, E_g the energy of the bandgap, k_B the Boltzman constant and T the temperature.

It is assumed that the n-doped layer is the top layer and the substrate is p-doped, this hypothesis is confirmed in section: III-C.

C. Measurement setup

For the measurements, samples of the solar cell are used instead of the complete cell, these are extracted using the Trotec speedy 300, a laser cutter. For the diode measurement, the samples are cut into a 20 [mm] ×20 [mm] square and for the TLM measurements, the sample size is 25 [mm] ×15 [mm]. The exact dimensions of the samples are given in Fig. 6. It is important to notice that the distance between probes for the TLM experiments is denoted by *d1, d2, d3, d4* and *d5*.

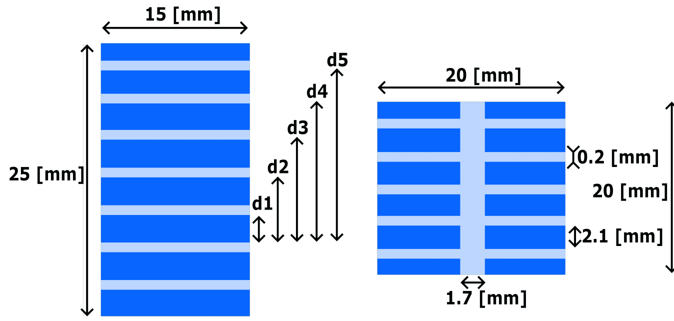

Fig. 6: Solar cell samples with corresponding dimension, on the left side the sample used in TLM measurements and on the right the sample for diode characterization.

The border of the samples are coarse which can be seen in Fig. 7.

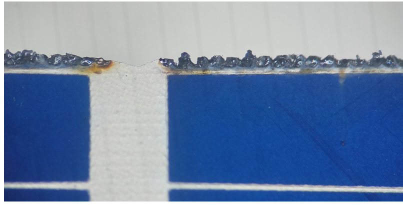

Fig. 7: Top view of the border of the diode sample, a visualisation on the coarse edges.

1) Transmission line method: To measure and characterize the contact and sheet resistance, the transmission line method (TLM) is used. By grounding the backplane and probing on top of the cell over two contacts the total resistance is measured [11]. The IV characteristics are found by applying a voltage sweep from -0.25 [V] to 0.25 [V] and measuring the current. The measurement setup is given in Fig. 8. Plotting the different total resistances found for each distance gives a linear relation from which R_C and R_{L1} can be found using eq. 10. Where R_C and R_{L1} are the contact and sheet resistance in [Ω], W is the distance between the probes in [m] and $R_{totalparastitics}$ is the parasitic resistance in [Ω]. The parasitic resistance can be subtracted as, duo to the orientation of the diodes, the non linear part of the circuit is neglected.

$$R_{total} = \frac{R_{L1}}{W}d + 2R_C + R_{totalparasitics} \quad (10)$$

Because of the diode orientation, it is assumed current only flows between Source Measuring Unit (SMU) 1 and SMU 2. It is assumed that the intermediate contact resitances (that for example contact 2 if probes are placed on contact 1 and 3) can be neglected as those should not significantly impact the measurement results.

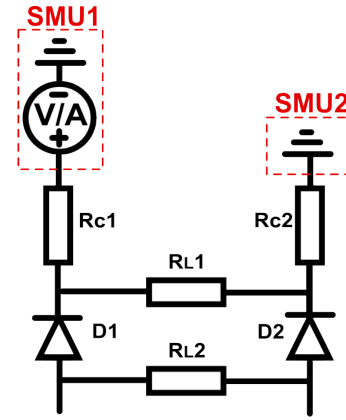

Fig. 8: Measurement set up for the transmission line method to characterize the sheet (R_{L1}, R_{L2}) and contact resistance (R_{C1}, R_{C2}).

Based on previous research and the recommendations given, are the probing pads connected to a solar cell sample with wire bonds which results in a more reliable probing location [2]. This way te distance to the border is kept constant and the probes do not influence the contact resistance by directly applying pressure on the silver contacts. In Fig. 9 these wire bond connections are seen. Fig. 9b shows the complete wafer during a measurement, where the parasitics of the wire bond are measured.

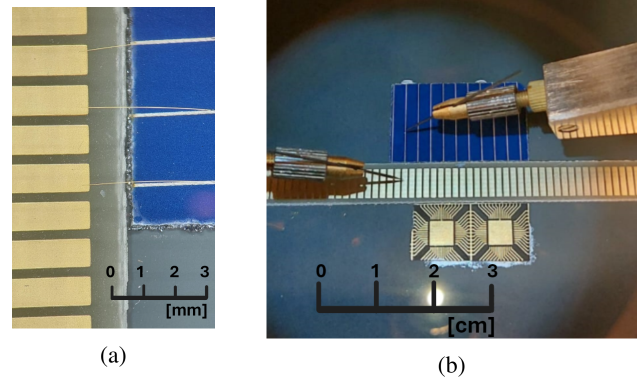

Fig. 9: (a) Wire bond connection from TLM sample to probing pads (gold), (b) Measurement setup in the Suss MicroTec PM300 Probe System with KE4200 using a probing pad for measuring the parasitic resistances of the wire bond.

2) Diode characteristics: To find the diode characteristics on the top of the cell a probe is placed and the bottom of the sample is connected to a ground plane, the measurement circuit is given in Fig. 10. SMU1 is the probe on top of the cell and the chuck is the ground plane connecting the bottom contact to ground. From the IV curves measured, the direction of the diode can be confirmed and other parameters such as the saturation current can be found.

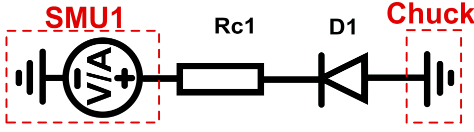

Fig. 10: Measurement setup to characterize the diode.

By varying the irradiation intensity when no voltage is applied and measuring over time, the current generation versus irradiation intensity can be measured. The solar simulator was not used for this but a simple lamp, that was available at the probing station. The light of this lamp does not correspond to the intensity and wavelengths as the sun, therefore this measurement will only be conducted to prove there is current generation in the cell.

3) Parasitics: To improve the quality of the data, parasitics like the resistance of the probes have to be taken into account. The probes will be placed on the same probing pad to measure the internal probe resistance, in Fig. 9a the probing pads are shown on the left side. For this measurement, it is assumed that the current will only flow from probe to probe and that the probing pad is not of any significance for the measurement result. Furthermore, is it assumed that no current flows towards the cell. Taking the inverse of the slope from the IV curve measurement, results in the resistance of the two probes together. For measuring the wire bond resistance one of the probes is placed on a probing pad where a wire bond is connected, the other probe is on the silver contact strips of the solar cell, where the other end of the wire bond is connected. This measurement setup is show in Fig. 9b. By applying a voltage sweep while measuring the current at the same time the IV characteristics can be determined. Using Ohm's law the resistance can be found. The resistance measured is over one wire bond including the two probes, to find the parasitic resistance of only one wirebond the resistance of the two needles needs to be subtracted.

The total parasitic resistance for the TLM measurement is given by eq. 11.

$$R_{totalparasitics} = 2R_{probe} + 2R_{wirebond} \tag{11}$$

For the diode measurements, the parasitic resistance assumed to be equal to the resistance of one probe as it is assumed the ground plane does not add any extra parasitic resistance and the probing pad does not contribute significantly to the result.

III. Measurements

Since the only known information about the cell is that the cell is made of silicon with an aluminium BSF measurements are carried out to characterize the contact resistance, sheet resistance, and diode parameters. When all component values are found, a simulation model is created in the LTSpice simulation software [13]. All measurements are carried out in the same environment with a room temperature of ± 24 $[^{\circ}C]$.

A. Parasitics

The IV curves of measuring over one wire bond and the measurement over just the probes are shown in Fig. 11. The compliance of the probing station limited measuring over larger ranges as it cut off the measurements at 0.1 [A]. Because of this limit not all data points could be used. The resistance is found from a linear approximation of these data points as the slope is the inverse of the resistance (eq. 12).

$$R = \frac{\Delta V}{\Delta I} = \frac{1}{Slope} \tag{12}$$

The parasitic resistance for the diode measurement is found to be 0.266 [Ω] and for the TLM measurement $R_{parasitic} = 1.09$ [Ω]. All of the following experiments were corrected for the offset caused by the parasitic resistances. The measurement for the probe resistance does not cross 0 [A] at a 0 [V] applied probably because of an offset caused by measurement inaccuracies.

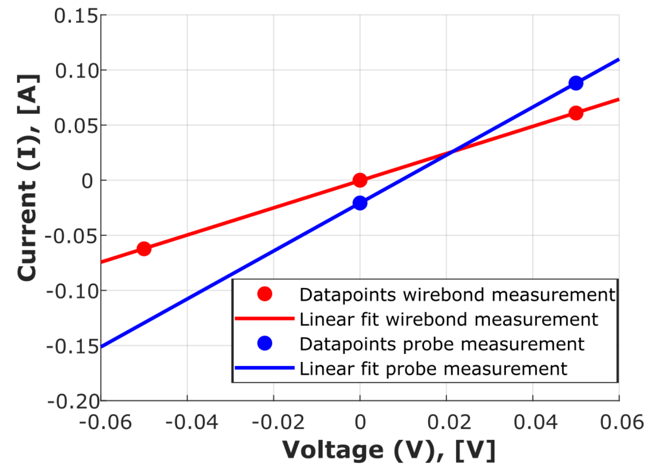

Fig. 11: Current versus voltage to characterize the parasitic resistances, measured without irradiation.

B. Transmission line method

In Fig. 12 the IV curves per probing distance are shown, from this plot the total resistance per distance can be found. All the measurements were conducted with 0% irradiation. Finding the resistance using eq. 12 and plotting this over the distance results in the plot given in Fig. 13. Using eq. 10 given in section II-C it is found that the contact resistance is 1.91 [Ω] and the sheet resistance of the top layer silicon between two fingers is 7.47 [Ω].

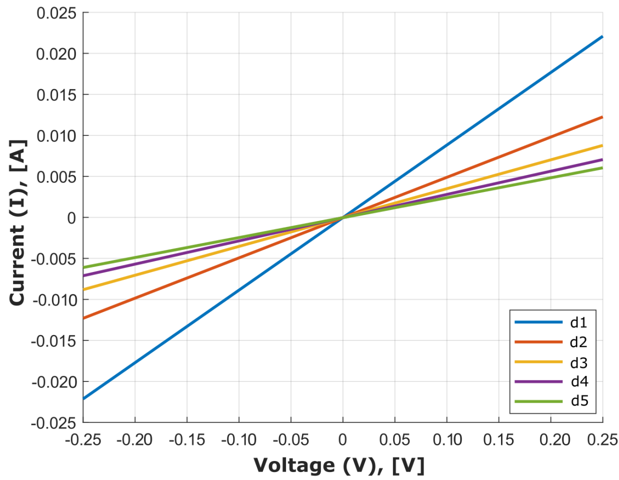

Fig. 12: Relation between current and voltage for each measured distance (*d1*-*d5*) on the TLM sample without any irradiation.

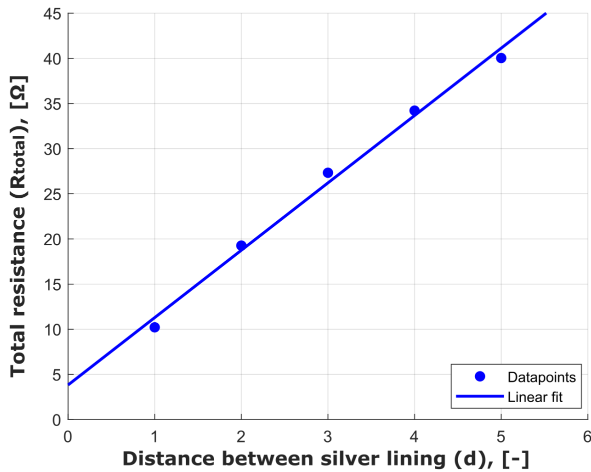

Fig. 13: Distance in probe placement (d) versus the total resistance (R_{tot}), found by taking the inverse of the slope of the IV curve as described in eq. 12.

The effective contact resistance (ρ_{c-eff}) is dependent on the area of the silver contact strips over which is measured. Eq. 8 may be used as the transfer lenght is found to be $\pm$1.08 [cm] which proves $W \leq 0.5L_T$ to be true. 0.057 $[\Omega \cdot cm^2]$ is found for ρ_{c-eff}. For the sheet resistance the amount of $\Omega/\square$ can be found, which is which is 53.4 $[\Omega/\square]$.

Inspecting Fig. 13 a slight curve can be observed, there appears to be a second-order component which is not taken into account in this first-order linear approximation.

The hypothesis is that R_C and R_{L1} are irradiation dependent the values for different irradiation intensities are plotted in Fig. 14. From these results, however, there does not seem to be an irradiation dependency in the resistances. The values of the measured contact resistances lie within 0.55% of the found 1.91 $[\Omega]$ over the range of the irradiation intensity (IRR). The maximum deviation calculated for the sheet resistance with respect to the average is 0.10%.

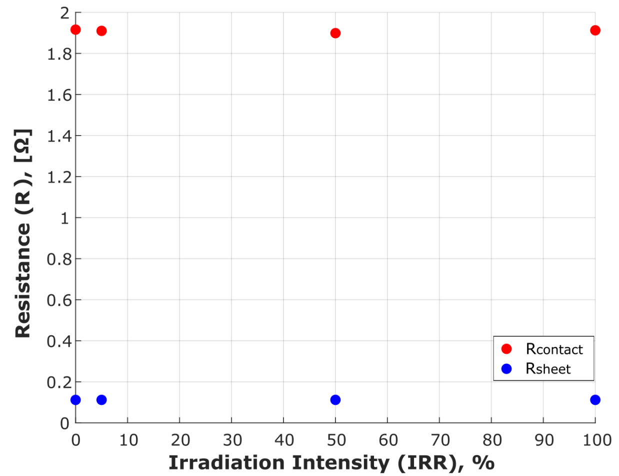

Fig. 14: The contact resistance and sheet resistance measured at d1 for different irradiation intensities.

C. Diode characteristics

The results of applying a voltage sweep over the diode sample can be seen in Fig. 15. For three different irradiation intensities, the IV curves are plotted. As shown in the left part of the graph the current exponentially decreases from -0.6 [V] to 0 [V]. The diode is ’open’ and current flows for a negative voltage difference compared to the ground. This confirms our hypothesis of the direction of the diode. The bulk is p-doped and the top layer is n-doped.

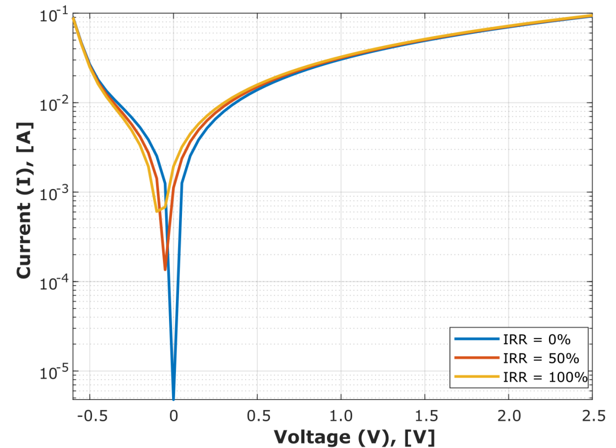

Fig. 15: IV characteristics for the diode measurement with the absolute value of I in logarithmic scale, three different irradiation intensities can be observed.

It is also immediately noticeable that the graph does not show the behaviour expected of an ideal diode. A probable cause of this is that there are extra current paths to the ground

caused by the imperfect edges of the sample (Fig. 7). The right half of the graphs shows approximately linear behaviour (seen in fig. 16) implying there is an extra resistance parallel to the diode creating a current path as the diode is not conducting.

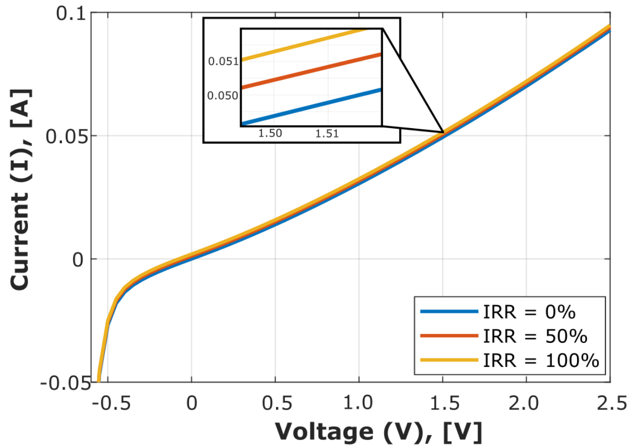

Fig. 16: IV characteristics for the diode measurement in linear scale, three different irradiation intensities can be observed.

The value of this parasitic resistance is approximately 25 [Ω]. This is found eq. 12 over the linear part of the measured IV curve (Fig. 16). Due to this extra current path, a value for the saturation current can not be found based on just measurement results. It is expected that this extra current path influenced the results of the TLM measurements slightly as the value of 25 [Ω] is substantially in the range of the sheet resistance measured resulting in a new current loop including the diode.

As more light is applied it is seen that the curves move upwards, implying more current is generated as irradiation intensities increase. This is confirmed by the following measurement, seen in Fig. 17, where no voltage is applied and only the current is measured as the light intensity increases.

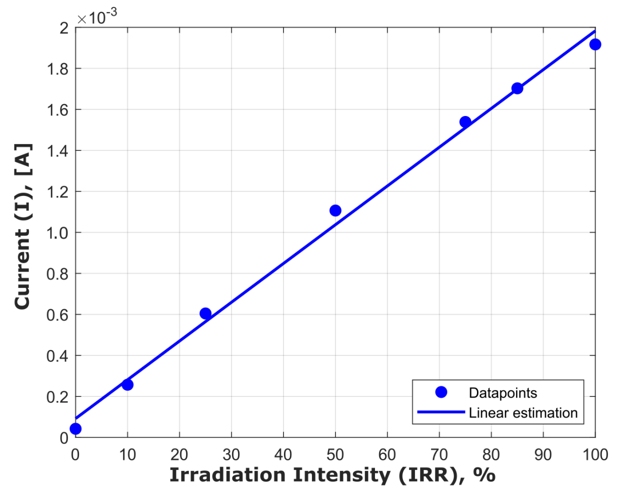

Fig. 17: Relation between the irradiation intensity on the sample and the current generated in the diode solar cell sample.

IV. Simulations

Based on the parameter values found in section III the solar cell is modelled. First, an ideal model is made after which the model is optimized closer to reality. Results that could not yet be explained in the measurement section are described based on model approximations. The software used to model is LTSpice [13].

A. Diode model

As concluded in the measurement section of the diode it is found that the diode does not behave as an ideal diode, this is most likely caused by unwanted current paths. In the LTSpice simulation software, a model is created with a diode and a parallel resistor of 25 [Ω]. The ideality factor (n), the saturation current (I_s), and the internal series resistance were iterated until there was a maximum difference between the simulation and measurement of 3.4 [mA]. The final values for the diode model are 1×10^{-10} [A] for I_s, a series resistance of 0.5 [Ω], and an ideality factor of 1.1. The comparison of an ideal diode model, simulation non-ideal diode model, and measurement can be seen in Fig. 18. For further simulations this new diode design is used and not the ideal one as this does not represent the behaviour observed from the measurements.

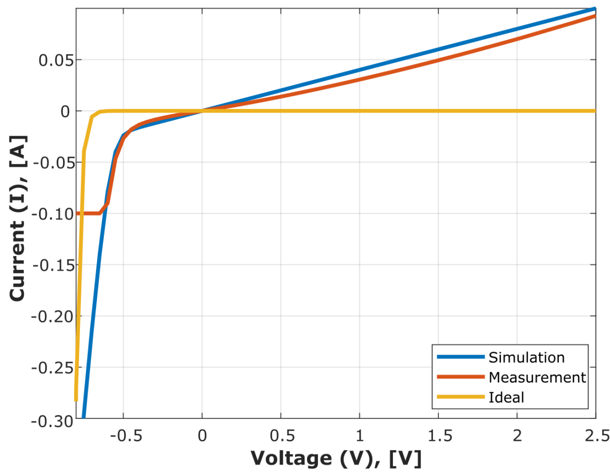

Fig. 18: Comparison of the IV characteristics of the ideal diode model (yellow), the diode model iterated to the actual measurement (blue) and the actual measurement (red) where simulation and measurement were without any irradiation.

B. Transmission Line Method

To correctly answer the question: 'What is the influence of irradiation and temperature on the behaviour of contact resistances comparing simulation and measurement?' simulations are compared to measurements for the transmission line method. First, the effect of shunt resistances is discussed, after which it is examined whether it is useful to extend the simulation circuit. Finally, the influence of irradiation is studied. The temperature influence can not be modelled as this depends too much the material properties of the doped silicon layers. LTSpice is capable of simulating temperature dependencies but not to this extent.

As was seen from fig. 13 there are influences of non linear components in the results of the TLM measurements. The difference between two following distances (that is from for example d1 to d2 or d3 to d4) is not constant since with an increasing distance the lines get closer to each other. A probable cause for this is introduction of shunt resistances. The shunt resistance, as found in previous section (IV-A), are ± 3.4 times bigger allowing a litle current to flow to the back side of the cell. This extra path causes the non linear behavior of the diode to show in the transmission line method results. The simulation results are compared to the measurement results in fig. 20, the in the dashed lines the simulation results are shown and the solid lines are the measurement results as shown before in fig. 12. The simulation is not perfect but the most dominant behavior is correct.

TABLE I: % difference in current over the contact resistance comparing the simulation to the measurement for each distance probed

d1	*d2*	*d3*	*d4*	*d5*
105.92%	118.91%	121.36%	119.20%	114.83%

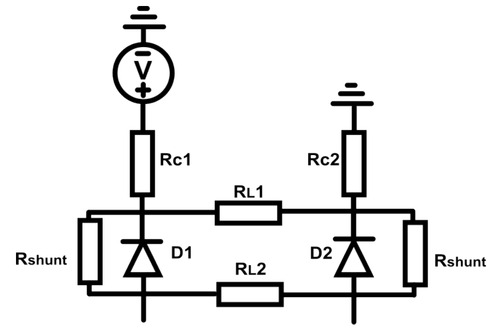

(a) Circuit diagram of the model used to simulate the TLM measurement with shunt resistances, the value of R_{L1} and R_{L2} changes based on the probing distance that is simulated.

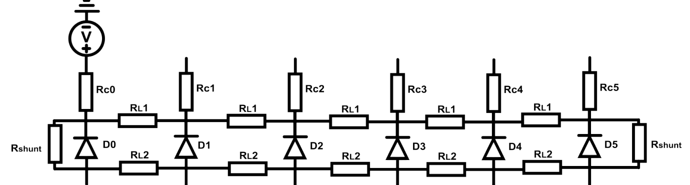

(b) Extended TLM measurement simulation model as an attempt to iterate closer to reality.

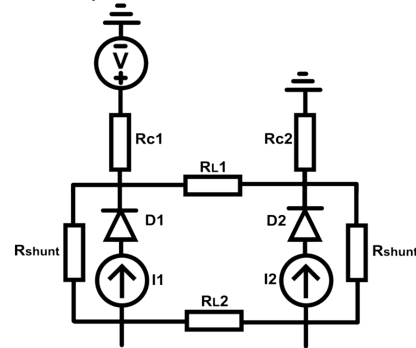

(c) Circuit diagram of the model used to simulate current generation in the TLM measurement, the value of R_{L1} and R_{L2} changes based on the probing distance that is simulated.

Fig. 19: Different iterations of the simulation model for TLM measurements.

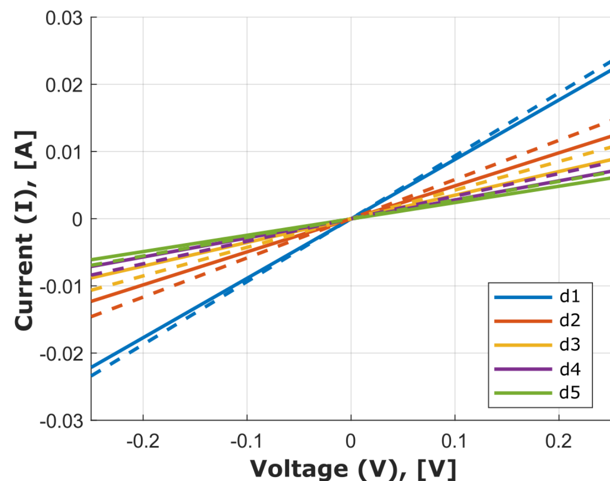

Fig. 20: Measurement (solid) and simulation (dashed) results for the current over the contact resistance for probing distance *d1* and *d5*. The TLM simulation circuit results are of a model with shunt resistance added and one without shunt resistance.

A possible explanation for the slight difference in current measured could be that the lumped element model is limiting the capability to model the behaviour correctly. For this reason, the model is extended as seen in Fig. 19b. Where the ground is connected to the contact resistance corresponding to the desired simulated TLM distance. However, after simulating for *d1-d5* it is found that this provides the same results. Also, the ratio between R_{L1} and R_{L2} does not significantly impact the TLM measurement, since barely there is barely any current in R_{L2} due to the diode orientation. Therefore the guess of 1:5 for $R_{L1} : R_{L2}$ is fine for a first-order approximation.

The current generated by light shining on a solar cell can simply be modelled as a current source, the circuit corresponding to this situation is given in Fig. 19c. When measuring it was found that irradiation did not affect the contact resistance. Using the equivalent model where the diode was optimized to fit the diode behaviour measured, it was found that, even though unexpected, the measurement results make sense. It turns out that the shunt resistances have a slightly increasing current as the current created by irradiation intensity increases. The low amount of current generated when the irradiation intensity was increased, was not high enough to overcome the measurement inaccuracies and compensate for the current in the shunt resistances. In Fig. 21 the simulation results, for $I_{generated}$ equals 1 [mA], 10 [mA] and 100 [mA], are shown. It is seen in the simulation that an increase in the produced current consequently increases the current measured at the contact resistance. This is seen as the IV curves moving upwards for higher generated currents by the current source. It can be concluded that contact resistances are in fact inversely proportional to the irradiation intensity, as, according to Ohms law, for a set voltage an increasing current results in a lower resistance.

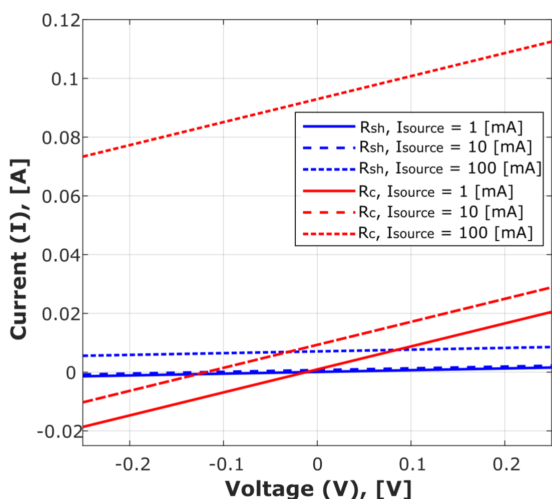

Fig. 21: Current through the shunt resistance and contact resistance for 1 [mA], 10 [mA] and 100 [mA] applied by a current source

V. Conclusion

In this research, contact resistances on silicon solar cells were characterized for irradiation and temperature changes based on the comparison of measurement and simulation. From the results, it is seen that irradiation does indeed affect the contact resistance. For higher irradiation intensities the current through the contact resistances is higher. The correlation between irradiation and resistance was not observed in the measurements possibly due to the introduction of shunt resistances and insufficient current produced by the light source that was used. The temperature influence was only theoretically found as the simulation software was not advanced enough to model semiconductor physical effects. There is an optimal temperature range for solar cells, as in this optimal range the internal material resistances are lowest, more research should be conducted to find this ideal range. Besides the influence of temperature, doping concentrations also significantly influence the resistive value of semiconductor layers and Schottky contact. An effect that was not taken into account in the analysis was the possibility of extra current paths. It is found that these extra resistances have a significant influence on the measured current. In the equivalent model of the solar cell it can be visualised the resistance creates an extra path to ground around the diode. These extra current paths also introduce second-order behaviour in the transmission line method results

A. Recommendations

Further research can include inspecting the second-order behaviour noticed in the IV graphs from TLM measurements and determining what physical phenomena occur for this curve to appear, as only a proof of concept is given.

If the focus is more on the irradiation aspect of the research an in-depth analysis can be done on the effect of the angle of irradiation. Also, more precise measurements can be executed finding a more precise relation between the current generated in a cell and the contact resistance measured. The temperature aspect can be elaborated by validating the theoretical hypothesis with measurements. More specialized simulation software can be used to model material physics to predict cell behaviour based on temperature variations.

If one is to repeat the same research the following recommendations, to improve the outcome can be given: first is minimizing the effect of the shunt resistance caused by the coarse edge of the sample. As explained in section II-C, a laser cutter was used to extract specific samples from the solar cell wafer. It could be seen that the edges of the retrieved samples were still really coarse. This contributed to the deviation between measurement and simulation. A new method to create wafer samples with cleaner edges could be developed, minimizing the effect caused by the parasitics introduced by the shunt resistance. Also, the number of assumptions, to simplify situations, can be reduced to improve the quality of the simulation results, this will result in more elaborate and complex models.

ACKNOWLEDGMENT

First I would like to thank Dr. Ir. C. Salm and Prof. Dr. J. Schmitz for being my supervisor during this thesis research. Their knowledge helped me learn a lot about this field of study and sparked my interest in doing research.

I would also like to express my gratitude to A. Attariabad, S.K. Kralj, and A. Dotsika for their introductory courses and guidance regarding the use of (measurement) equipment. Also a special thanks to A.R. Rop for helping create a wafer that could be used to improve measurement accuracy. Lastly, I am also thankful for my friends who helped me get a different perspective on problems and their support during my thesis.

AI STATEMENT

During the writing of this thesis, ChatGPT was used to create MATLAB scripts for specific actions, like creating a first-order approximation based on data points. The language tool Grammarly was also used to help with scientific writing and the use of synonyms. The author reviewed all the outcomes and adjusted everything as needed. The author takes full responsibility for the content of this paper.

REFERENCES

[1] Centraal Bureau voor de Statistiek. (June 2024) Energieverbruik uit hernieuwbare bronnen gestegen naar 17 procent. [Online]. Available: https://www.cbs.nl/nl-nl/nieuws/2024/23/energieverbruik-uit-hernieuwbare-bronnen-gestegen-naar-17-procent

[2] H. Gün, *Effect of Irradiation on Transmission Line Method Measurements on Silicon Solar Cells*. EEMCS, July 2024. [Bachelor's thesis, Univesity of Twente].

[3] C. Nijland, *Analysing the Effect of High-level Irradiation on Contact Resistance in Solar Cells*. EEMCS, August 2024. [Bachelor's thesis, Univesity of Twente].

[4] F. Ghani, G. Rosengarten, M. Duke, and J. Carson, "On the influence of temperature on crystalline silicon solar cell characterization parameters," *Solar Energy*, vol. 112, pp. 437–445, february 2015.

[5] E. Radziemska and E. Klugmann, "Thermally affected parameters of the current-voltage characteristics of silicon photocell," *Energy Conversion and Managment*, vol. 43, pp. 1889–1900, September 2002.

[6] X. Gu, X. Yu, and D.Yang, "Efficiency improvement of crystalline silicon solar cells with a back-surface field produced by boron and aluminum co-doping," *Scripta Materialia*, vol. 66, pp. 394–397, March 2012.

[7] Unknown. TUGraz. Pht.301 physics of semiconductor devices, electrical conductivity of silicon. [Online]. Available: https://lampz.tugraz.at/~hadley/psd/L4/conductivity.php

[8] ——. Pht.301 physics of semiconductor devices, electron and hole mobility of silicon. [Online]. Available: https://lampz.tugraz.at/~hadley/psd/L4/mobility.php

[9] S. Elfiky, M. Zahran, A. Kassem, A. Eliwa, and A. Fargal, "A study on the impact of pn-junction doping concentration on the efficiency of monocrystalline silicon solar cells," *Sohag Engineering Journal*, vol. 3, September 2023.

[10] R. Hueting, A. Mouthaan, J. Schmitz, and G. Sasse, *Semiconductor Devices Explained More*. p130-p135: University of Twente, 2018.

[11] D. K. Schroder, *Semiconductor Material and Device Characterization, Chapter 3*, 3rd ed. p133-p147: A Wiley-Interscience Publication, 2005.

[12] Unknown. California Polytechnic State University. Solid state physics laboratory, experiment 15: Temperature dependece of the saturation current of a juction diode. [Online]. Available: https://www.reed.edu/physics/332/pdf/Saturation_Current.pdf

[13] Analog Devices. Ltspice. [Online]. Available: https://www.analog.com/en/resources/design-tools-and-calculators/ltspice-simulator.html